Near-infrared counterparts of Chandra X-ray sources toward the Galactic Center

Curtis DeWitt[1], Reba M. Bandyopadhyay[1], Stephen S. Eikenberry[1,2], Robert Blum[3,5], Knut Olsen[3], Kris Sellgren[4] and Ata Sarajedini[1]

dewitt@astro.ufl.edu

ABSTRACT

The *Chandra* X-ray Observatory has now discovered nearly 10,000 X-ray point sources in the $2^\circ \times 0.8^\circ$ region around the Galactic Center (Muno et al. 2009). The sources are likely to be a population of accreting binaries in the Galactic Center, but little else is known of their nature. We obtained JHK_s imaging of the $17' \times 17'$ region around Sgr A*, an area containing 4339 of these X-ray sources, with the ISPI camera on the CTIO 4-m telescope. We cross-correlate the *Chandra* and ISPI catalogs to find potential IR counterparts to the X-ray sources. The extreme IR source crowding in the field means that it is not possible to establish the authenticity of the matches with astrometry and photometry alone. We find 2137 IR/X-ray astrometrically matched sources: statistically we estimate that our catalog contains 289 ± 13 true matches to soft X-ray sources and 154 ± 39 matches to hard X-ray sources. However, the fraction of true counterparts to candidate counterparts for hard sources is just 11 %, compared to 60 % for soft sources, making hard source NIR matches particularly challenging for spectroscopic follow-up. We calculate a color-magnitude diagram (CMD) for the matches to hard X-ray sources, and find regions where significant numbers of the IR matches are real. We use their CMD positions to place limits on the absolute K_s band magnitudes of the potential NIR counterparts to hard

[1]University of Florida

[2]University of Florida Research Foundation Professor of Astronomy

[3]National Optical Astronomy Observatories, Tucson, AZ 85719

[4]Ohio State University

[5]Visiting astronomer, Cerro Tololo Inter-American Observatory, National Optical Astronomy Observatory, which are operated by the Association of Universities for Research in Astronomy, under contract with the National Science Foundation.

X-ray sources. We find regions of the counterpart CMD with 9 ± 3 likely Wolf-Rayet/supergiant binaries (with 4 spectroscopically confirmed in the literature) as well as 44 ± 13 candidates that could consist of either main sequence high mass X-ray binaries or red giants with an accreting compact companion. In order to aid spectroscopic followup we sort the candidate counterpart catalog on the basis of IR and X-ray properties to determine which source characteristics increase the probability of a true match. We find a set of 98 IR matches to hard X-ray sources with reddenings consistent with GC distances which have a 45% probability of being true counterparts.

Subject headings: Galaxy: center - infrared: stars - X-rays: stars

1. Introduction

The Galactic Center (GC) has been the target of several major observing campaigns with the *Chandra* X-ray Observatory. One of the primary results of these campaigns has been to unveil numerous faint and spectrally hard X-ray point sources toward the GC region. Hard X-ray sources, with spectral energy distributions (SEDs) that peak above 1.5 keV, often arise from high extinction. Wang et al (2002) uncovered $\sim$ 1000 such point sources in a $2^o \times 0.8^o$ field while searching for the source of the He-like Fe emission emanating from the GC. To investigate the nature of these point sources, Muno et al. (2003a) reobserved the central $17' \times 17'$ around Sgr A* for an additional 590ks, increasing the total observing time to 626 ks and the number of X-ray point sources to 2357. More than 2000 of the sources were undetected below 1.5 keV, indicating a large amount of extinction. The line-of-sight to the Galactic Center has an average column density of $N_H = 6 \times 10^{22}\ cm^{-1}$ (Baganoff et al. 2003), which causes the flux below 1.5 keV to experience more than $\tau = 2$ of attenuation (Tan & Draine 2004). This suggests that the hard X-ray sources with attenuated emission below 1.5 keV lie at or beyond the GC distance.

The faintness and hardness of the X-ray emission from these sources could in theory be met by background active galactic nuclei (AGN), but Bandyopadhyay et al. (2005) find that the number of background AGN within the $2^o \times 0.8^o$ field is $< 10\%$, using the source count distributions from the *Chandra* Deep Field extragalactic surveys. Muno et al. (2003a) perform a similar analysis of the number of background AGNs in the smaller $17' \times 17'$ field and find that between 20-100 of the 2076 X-ray sources detected at energies above 2keV are AGN, meaning that the bulk of the hard X-ray sources lie within the Galaxy near to or beyond the GC distance.

Muno et al. (2003a) enumerate the possible classes to which these unidentified X-ray sources may belong; these include coronally active main sequence stars, Young Stellar Objects (YSOs), Algol binaries, Wolf-Rayet stars (WRs), cataclysmic variables (CVs), pulsars, low mass X-ray binaries (LMXBs) and high mass X-ray binaries (HMXBs). The soft foreground X-ray sources could in theory belong to any of these classes based on their X-ray SEDs; however their low X-ray luminosity suggests that they may be more likely to be CVs or coronally active single stars. Of these candidate source types, only LMXBs, HMXBs and a subclass of CVs with high magnetic fields called Intermediate Polars (IPs) are known to produce enough hard X-rays to be detectable through the large extinction to the GC.

Muno et al. (2003b) search for X-ray flux variability of the sources in the Muno et al. (2003a) X-ray point source catalog. They detect 8 sources with periodic variability among the brightest X-ray sources, but the vast majority of sources are too faint to search for flux variability at similar levels.

The next step in identifying the nature of the X-ray sources is to search for them at other wavelengths. The near-infrared bandpass is well suited to this effort because stellar photospheres are bright in these bands and the average extinction is dramatically less than at optical pass-bands. However, source crowding makes definitive association between X-ray and IR sources difficult. For example, a 1" radius circle at a random location within $10'$ of Sgr A* would contain a $K_s < 14.5\ mag$ star more than 25 % of the time and this percentage only increases with fainter magnitudes. Thus, the authenticity of an individual IR/X-ray match can only be verified through spectroscopy. However, one can also examine the astrometrically identified candidate counterparts as a group, and make statistical arguments as to the presence and possible nature of true counterparts within the catalog of matched sources.

Several groups approach this problem by calculating the excess in the number of X-ray/IR matches over the number expected by random coincidence, including Bandyopadhyay et al. (2005), Laycock et al. (2005), Arendt et al. (2008), Gosling et al. (2009) and Mauerhan et al. (2009). Bandyopadhyay et al. (2005) used ISAAC on the VLT to image fields containing 77 of the X-ray point sources discovered by Wang et al (2002). They detect a small excess in counterparts in the J and H bands, but find no significant excess in matches in the K band. However, the positions of a number of the X-ray sources in the first *Chandra* source catalog were found be inaccurate at the 0.5" level. A reanalysis of the X-ray/IR matching of these data sets after the X-ray astrometry was improved indicates a 2-3 σ excess in detections over that expected from random chance in J,H and K bands (Gosling et al. 2010).

Laycock et al. (2005) observe the central $10' \times 10'$ GC area with the PANIC near-infrared camera on Magellan to a confusion limit of $K_s = 15.4\ mag$. Cross-correlating their IR catalog

to the X-ray catalog of Muno et al. (2003a), they find a strong IR/X-ray matching significance for the soft X-ray sources, but little significance for the hard X-ray sources. They calculate that no more than 10 % of the hard X-ray point sources can have apparent K_s magnitudes brighter than 15 mag. Assuming these hard X-ray sources reside in the GC, they conclude that certain types of X-ray binaries that have bright mass-donor stars, such as Be-neutron HMXBs, must contribute no more than 10 % to the hard X-ray source numbers.

Arendt et al. (2008) perform similar matching simulations using a catalog of $\sim$ 20000 *Spitzer* IRAC point sources detected at $\lambda = 3.6, 4.5, 5.8$ and $8.0 \mu m$ lying within the $17' \times 17'$ field of the Muno et al. (2003a) *Chandra* observations. They found that the soft X-ray sources are correlated to the IRAC catalog, but they detect no such correlation to the hard X-ray sources. However, they note that source crowding limits their catalog to Galactic center sources with $[3.5] < 12.4\ mag$, and actual counterparts may be much fainter than this limit.

Since these studies were published, the Galactic Center X-ray point source catalog has been updated to include a total of 2 Ms of accumulated observations of the $2^\circ \times 0.8^\circ$ area around Sgr A* (Muno et al. 2009). 9017 X-ray point sources are detected, the positions of many of which have been refined from the earlier catalogs. The majority of the sources in the catalog have astrometric errors less than 0.7". Mauerhan et al. (2009) utilize this data together with near-infrared data from the SIRIUS camera on the 1.4m telescope at Sutherland Observatory in South Africa, and present a catalog of 5184 potential near-infrared candidate counterparts to the X-ray sources. They find that, statistically, 394 of the NIR matches to the hard X-ray sources are real counterparts. This amounts to 5.8% of the 6760 hard X-ray sources, consistent with the findings of Laycock et al. (2005) which limit this percentage to no more than 10%.

A complete accounting of the fraction of low mass X-ray binaries (LMXBs) and high mass X-ray binaries (HMXBs) can provide a useful tracer of both the accumulated star formation and the ongoing star formation in the GC (Grimm et al. 2003). The search can also yield rare and important systems, such as microquasars, X-ray pulsars, and wind-colliding binaries. Mikles et al. (2006), Hyodo et al. (2008) and Mauerhan et al. (2010) have discovered possible wind-colliding O supergiant and Wolf-Rayet binaries in the GC. These systems could prove to be important laboratories for studies of high-mass stellar winds and it may be that more sources of this rare type will be found amoung the GC X-ray population.

The only way to positively identify individual sources is with spectroscopy. In the near infrared, active accretion manifests in emission lines, such as in Brγ line emission. Spectroscopic campaigns such as those described in Mikles et al. (2006), Mauerhan et al. (2010) and Gosling et al. (2010) have observed only the brightest infrared matches to X-ray

sources. With the coming advent of deep multi-object spectroscopy in the near-infrared (Eikenberry 2008), it will be possible to comprehensively follow up nearly all potential near-infrared counterparts, greatly increasing the chance of discovering the true nature of these X-ray populations.

In this work, we present new NIR imaging of the deepest part of the *Chandra* observations in the $17' \times 17'$ area around $SgrA^*$ containing 4339 X-ray point sources. We create a catalog of 2137 candidate NIR counterparts to X-ray point sources and statistically identify the locations of the true counterparts on a NIR color-magnitude diagram. We also isolate the characteristics that make likely authentic counterparts easier to find amongst the large number of spurious matches. These results will greatly aid the target selection for future spectroscopic observations as well as indicating the likely types of interacting binaries we may identify within this source population.

2. Observational Data

We use four sets of data in this work: the *Chandra* X-ray point source catalog of Muno et al. (2009), a near-infrared *J*,*H* and K_s catalog from our observations with ISPI at the CTIO 4m telescope, the 2MASS JHK_s all sky data release (Skrutskie et al. 2006), and the *JHK* imaging data and catalogs of the UKIDSS Galactic Plane Survey (Lucas et al. 2008). The 2MASS and UKIDSS data were used to photometrically and astrometrically calibrate the ISPI data, while the ISPI data and *Chandra* data were used to create a crossmatched source catalog.

2.1. X-ray

Muno et al. (2009) compile 88 *Chandra* observations of the Galactic Center (GC) taken between April 2000 and August 2007 and find 9017 point sources over a $2^\circ \times 0.8^\circ$ field. The $17' \times 17'$ field centered on Sgr A* has been the target of 1Ms of exposures and has some of the best sensitivity (4×10^{31} ergs s^{-1} for GC sources at 8 kpc distance) and the best positional accuracy in the X-ray catalog. 76 % of the X-ray sources in this region have positional accuracies of $0.7''$ and better.

2.2. ISPI

We used the ISPI camera on the CTIO 4m Blanco Telescope to observe the $17' \times 17'$ central region of the GC, covering the region of highest source density and in sensitivity in the *Chandra* X-ray data. ISPI has a $10.5'$ square field of view and a $0.3''$/pixel plate scale (van der Bliek et al. 2004). We observed the $17' \times 17'$ region with the J, H and K_s filters, on August 10, 2005.

We obtained IR imaging of the full *Chandra* field of Muno et al. (2003a) using a total of 4 pointings. The individual exposure times were short, 3.2s for H and K_s and 5s for J, so that the number of saturated bright sources would be kept to a minimum. We used a 5 point dither pattern with a nod length of 20" to compensate for the detector's cosmetic defects. The total exposure times for each quadrant of the field were 200s, 113s and 32s for J, H and K_s, respectively. Between pointings we checked the image focus by observing the center of the field. The focus stability was very good, which allowed us to use these frames for the creation of a fifth pointing, overlapping the other 4 pointings. This amounted to obtaining an additional frame with exposure times of 60s, 68s and 68s for the J, H and K_s filters. The typical seeing for all images was $\sim 0.9''$. The theoretical limiting magnitudes (not including crowding effects) for the fields were J= 19.5 mag, H= 18.5 mag, and K_s= 17.7 mag, taken from the CTIO exposure calculator for ISPI. For sky background removal we observed an offsource field 10 degrees south of the GC, with the same exposure times and the same 5 point dither pattern in all 3 filters. Dome flats and dark frames were taken at the beginning and end of the night. The left panel of Figure 1 shows a 3-color composite image of the full $17' \times 17'$ field and demonstrates the extreme stellar crowding in this region. The right panel of Figure 1 displays the pointing pattern of our observations.

2.3. 2MASS data

The 2MASS catalog is an all-sky J, H and K_s survey that has become a standard infrared photometry reference (Skrutskie et al. 2006). The astrometric precision of 2MASS is reported as $\sim 0.15''$ RMS. We used this catalog for calculating the ISPI image distortion and defining the WCS of the images. However the depth of the survey is significantly shallower than the ISPI data, with 10σ limits of J= 15.8 mag, H= 15.1 mag and K_s= 14.3 mag and a point spread function (PSF) full width half maximum (FWHM) which was typically between 2.5" and 3". The severe crowding in the GC makes the "effective" magnitude limits even brighter than these nominal values. The combination of the high crowding and larger PSF of 2MASS meant that many stars that could have been used as photometric references for our ISPI field were badly blended in 2MASS.

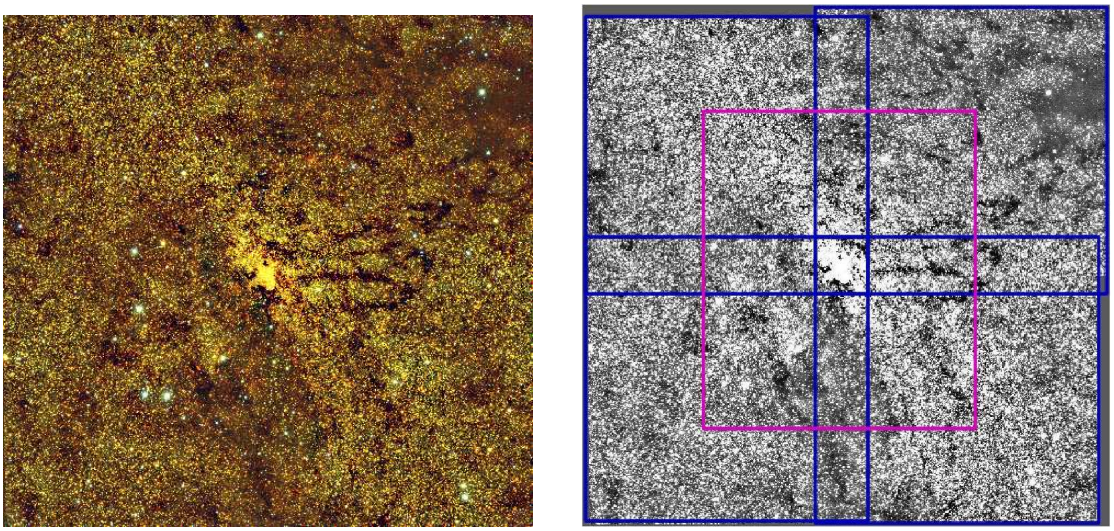

(a) (b)

Fig. 1.— (left) 3 color JHK_s composite image of ISPI Galactic center data. Each side is 17' in length. North is up and east is to the left. (right) The pointing pattern of the ISPI observations, overlaid on the K_s image. The magenta box represents the $10.5' \times 10.5'$ field of view of a single pointing with ISPI. The full frame is a $17' \times 17'$ region and consists of 5 such pointings.

2.4. UKIDSS Data

The UKIRT Infrared Deep Sky Survey (UKIDSS) is a set of 5 NIR imaging surveys with complementary goals (Lawrence et al. 2007). One of the subsurveys is the Galactic Plane Survey (GPS), which includes *JHK* coverage of the region between $-5° < l < 15°$ and $|b| < 2°$ (Lucas et al. 2008). The nominal survey depth was J= 19.9 mag, H= 19.0 mag and K= 18.8 mag. The plate scale of the UKIRT IR camera is 0.4", but using the technique of microstepping the delivered plate scale of the images is 0.2". The typical seeing is 0.9" for the data covering the region of our ISPI field. The primary data product of the survey is a source catalog produced with an aperture photometry pipeline. We rederived the photometry of UKIDSS GC data with PSF-fitting in DAOPHOT, in part to better match the PSF photometry that we performed with ISPI and in part because the aperture pipeline catalogs did not include some of the highest stellar density regions in the field. The details of the UKIDSS PSF reduction followed the same procedures as for ISPI PSF reduction, described in §3.1, and will be described in full in a subsequent paper (DeWitt et al., in prep.). The *JHK* filter set for the UKIDSS survey is slightly different from the JHK_s set used by 2MASS and ISPI. We converted the UKIDSS *JHK* magnitudes to the 2MASS system using the

prescription found in Hodgekin et al. (2009). The depth and resolution of the UKIDSS data are a closer match to the ISPI data than 2MASS, allowing better star-to-star comparison of the photometry. We used our PSF-fit UKIDSS catalog along with the 2MASS catalog for photometric calibration of the ISPI data.

3. Data Reduction

3.1. Creating the ISPI catalog

The ISPI images were reduced with the FATBOY pipeline, an imaging and spectroscopy package developed at University of Florida (Warner et al. 2010). FATBOY uses Python routines similar to the standard image reduction tasks found in IRAF. The processing steps include pixel linearization, dark subtraction, flat-field correction, cosmic-ray removal, sky-background subtraction and image stacking. We made a 6^{th} order distortion correction for each color using the 2MASS data, and used it to stack images in each color and pointing into an image of uniform plate scale. At this stage we had 5 images in each filter covering the full $17' \times 17'$ field.

The surface density of detected point sources was very large: 0.03, 0.25 and 0.25 sources/arcsec^2 for *J*,*H* and K_s, respectively. These densities were unsuitably large for standard aperture photometry, and we therefore employed DAOPHOT and ALLSTAR, which are specially designed for crowded fields (Stetson 1987), to perform PSF-fitting photometry on each of the stacked images.

We locked the astrometry to the 2MASS catalog by using the IRAF task *MSCTPEAK*. The residual RMS error of the ISPI plate solution with respect to *2MASS* was 0.2". The internal astrometric precision of 2MASS is reported to be 0.15" (Skrutskie et al. 2006). We used the 2MASS catalog to find photometric zeropoints for each image, by positionally matching the bright, unblended 2MASS sources to stars found in the 2MASS catalog and then calculating the median offset. At this point we had five catalogs for each filter, one for each ISPI pointing, with significant overlap in coverage between the catalogs.

We merged the per-pointing ISPI catalogs of each filter using a 0.3" error radius. We combined the catalog entries by either averaging the photometry, or in the case where the same star differed in brightness by more than the 1σ error for that magnitude (see §3.2), we adopted whichever brightness measurement had the lower PSF fitting residuals reported by *DAOPHOT*. The result was a single catalog for each of the *J*, *H* and K_s filters, covering the entire $17' \times 17'$ ISPI GC field.

We merged the J, H and K_s catalogs into a single three color catalog by matching sources between the individual filters with a 0.3" error radius. The standard deviation of the positions of sources matched across filters is ~ 0.1", which means our 0.3" match threshhold should match sources with up to 3σ positional errors. First the J, H and K_s catalogs were matched in pairs, i.e. JH,JK_s and HK_s. To locate the 3-filter matches we identified entries from the JH catalog and HK_s catalog with the same H band source. Fewer than 0.5% of sources had multiple astrometric matches in another band. In the few cases when there was a second astrometric match, we adopted the closer match for our final merged catalog. We used the K_s band position whenever available for the final catalog astrometry. If a source was not detected in K_s, we used the H position, and if H was unavailable we used the J position.

The final catalog contains 241,552 distinct sources, consisting of 50,851 detections in J, 200,302 detections in H and 192,292 detections in K_s. The reason for the greater number of detections in H than in K_s is mostly due to $\sim 24,000$ arcsec^2 of missing coverage in the K_s band on the outer parts of the observed fields. These areas were observed in K_s as part of the dither pattern of one of the pointings, but they were discarded because two K_s images were blurred by telescope shake. This region with only J and H band coverage lies on the outer edges of the North-East quadrant of 1 and makes up just $\sim 2\%$ of the total $17' \times 17'$ area of the ISPI GC field.

3.2. Photometric errors and completeness

To derive photometric errors we used regions of the field that were observed multiple times in the ISPI data. We calculated the differences in the measured magnitudes, and took the standard deviation of all stars in a certain magnitude bin to represent $\sqrt{2}\times$ the error for that magnitude. This error should encompass photon noise and errors associated with PSF-fitting, but it will be an underestimate when stellar blending dominates the noise. The error versus magnitude relation for each filter is shown in the left panel of Figure 2.

We calculated the completeness fraction of our catalogs by injecting artificial stars of various magnitudes into the images with the DAOPHOT tool *addstar*. The stars were overlaid on the original images in a sparse rectangular grid where the magnitudes and x and y values of the grid position were randomly assigned. We made sure that the magnitude range covered the interval where between 1% and 95% of stars were recovered. We restricted the number of injected stars to fewer than 10 % of the number of stars already contained in the image in order to prevent the introduction of different crowding characteristics. The *DAOPHOT* and *ALLSTAR* parameters were kept the same as in the original reduction. We

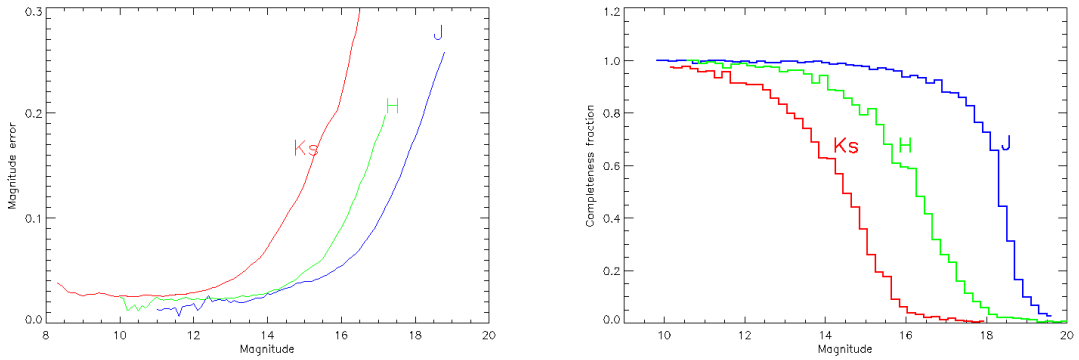

(a) (b)

Fig. 2.— (left) ISPI Photometric Error: Error per filter derived using multiple measurements of the same stars. (right) ISPI photometric completeness: The fraction of artificial stars recovered at a given J,H or K_s magnitude.

counted an artificial star as recovered if it was found within 0.5" of its injected position and we excluded any artificial stars that fell within 0.5" of a real star in the ISPI images. Figure 2 shows the completeness fraction versus magnitude for artificial stars for the J, H, and K_s filters. These values should reflect typical regions in the ISPI field, but the local completeness limit will likely vary with the source density changes across the field.

In Table 1 we show the number of sources in the final merged ISPI catalog, the 5σ limiting magnitude predicted by the ISPI exposure calculator from Poisson statistics, the 5σ magnitude limit (where the magnitude error is ~ 0.2 mag) calculated from the photometry of stars observed multiple times, and the mean 50 % completeness magnitude for each of the filters.

Table 1: ISPI point source catalog characteristics.

Filter	Number of stars	5-σ Mag. limit, Poisson error	5-σ Mag. limit, fitting error	50% Completeness limit
J	50851	19.5	18.3	18.4
H	200302	18.7	17.2	16.4
K_s	192292	17.3	15.8	14.5

4. Real and spurious IR matches to the Chandra X-ray catalog

There are 4339 X-ray point sources from the Muno et al. (2009) catalog that lie within our field. We exclude any X-ray sources with $\sigma_X > 2.0$", where σ_X is the 95% positional uncertainty for the X-ray sources, in arcseconds. The 71 sources with larger errors have a median number of possible matches of 5 each, which would preclude useful follow-up. For the rest of this work we only consider the remaining 4268 X-ray sources.

We cross-correlate these 4268 X-ray sources with the ISPI catalog using a $\sigma_X + 0.2$" matching radius, where 0.2" represents the IR catalog astrometric error. We do not use the quadrature sum of these errors, $\sqrt{\sigma_X^2 + 0.2^{2}"}$, because it underestimates our positional uncertainty. The imperfect distortion correction contributes a small, regional systematic error to the 0.2", which we discovered during the filter merging stage of the ISPI catalog creation. This type of error should have an additive effect on the separation between X-ray and NIR sources. This matching criterion is imperfect, and may exclude a small number of actual NIR/X-ray matches with $\sim 3\sigma$ positional errors, but we have compromised in order to obtain fewer spurious matches so that we can extract useful information from the matched sources.

With this matching criterion in effect, we find that 43.2% of X-ray sources have 1 or more candidate NIR counterparts within their matching radius, and 5.5% have 2 or more counterparts (see Table 2). Our catalog of ISPI/X-ray matches is available online as a searchable database called *Chandra Galactica*. The website url is http://galcent.astro.ufl.edu. A sample of the catalog is shown in Table 9.

In Figure 3 we show magnitude and color histograms for all the ISPI sources and the candidate matches to X-ray sources. The histogram for the X-ray candidate counterpart IR sources is overplotted in red and normalized to the total number of sources in the whole ISPI catalog. Inset in each histogram is the same data plotted as a cumulative distribution. The J band clearly shows a difference between the candidate counterparts and the field

Table 2: Number of X-ray sources with 0,1,2, or > 3 astrometric matches in the ISPI JHK_s catalog.

Number of Matches	Occurences	Percentage
0	2425	56.8%
1	1610	37.7%
2	192	4.5%
>3	41	1.0%

source populations. The fact that the distribution of the J band magnitudes of candidate counterpart is distinct from the entire catalog suggests that at least some of these matches are real. The H and K_s candidate counterpart magnitude distributions are less distinct from the overall ISPI catalog, which is probably due to the higher rate of spurious matches in these bands.

The $(J-H)$,$(J-K_s)$ and $(H-K_s)$ color histograms in the lower panels of Figure 3 all clearly show an excess in matches to less reddened foreground sources. This suggests that a significant number of the unreddened candidate counterparts to X-ray sources are authentic counterparts.

In Figures 4 and 5 we display a H-K_s/K_s CMD and a J-H/H-K_s color-color diagram of the matched NIR sources and the entire ISPI catalog. The CMD clearly shows 2 populations of sources: sources with low reddening in a nearly vertical line at H-K_s= 0.2 mag and sources with high reddening centered at H-K_s= 2.0 mag. The sources with low reddening are nearby field sources, while the sources with high reddening should be near the GC. The color-color diagram shows that the sources are dispersed along the reddening vector. By eye, the X-ray source matches marked in color on these figures show little difference from the overall ISPI catalog. This would be expected either if the sources actually are not distinct from the overall NIR source population or if most of the matches are spurious. To evaluate the number and characteristics of the probable true matches, we need to have an idea of the number of matches that would happen simply by chance.

4.1. Definitions of the catalog properties

We divide the matched catalog into properties of the X-ray and IR sources in order to calculate the number of true physical counterparts with a given set of IR/X-ray properties. The X-ray characteristics include σ_X, the X-ray source positional error, in arcseconds; the X-ray hardness ratio; the X-ray luminosity; and the number of IR sources in the vicinity of the X-ray source.

1. Positional Error Sources with smaller X-ray error circles are likely to have fewer coincidental matches. In the left panel of Figure 6 we show the histogram of position errors for the 4268 X-ray sources with positional uncertainties under 2" and for the 1864 X-ray

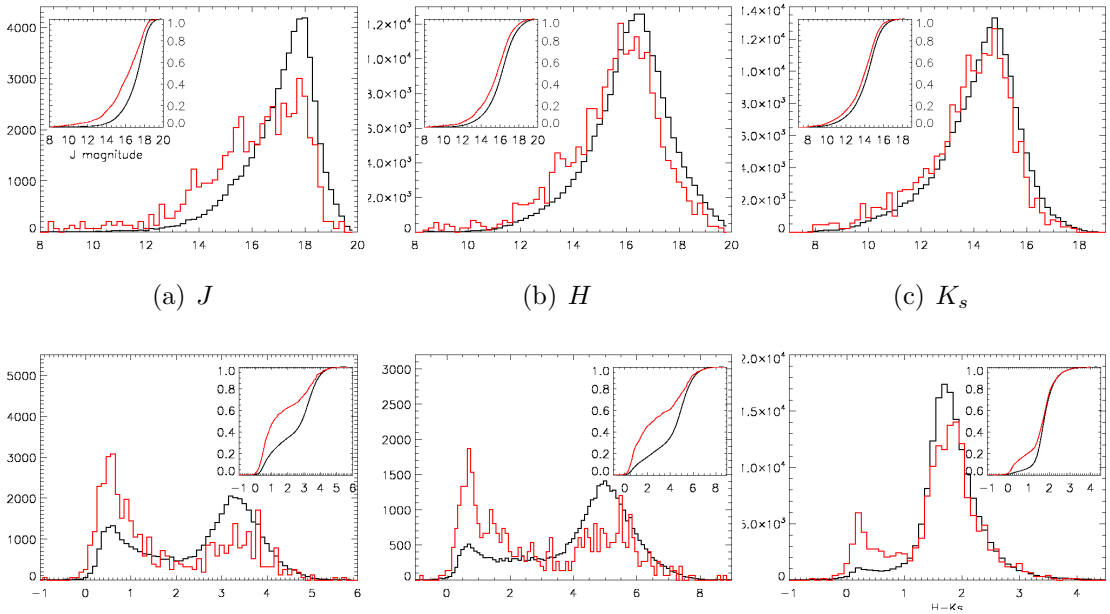

(a) J (b) H (c) K_s

(d) $(J-H)$ (e) $(J-K_s)$ (f) $(H-K_s)$

Fig. 3.— Magnitude and color histograms and cumulative distributions for all sources in the ISPI IR catalog (in black) and for just the IR source matches to X-ray sources (in red). The histograms for the X-ray matched IR sources are normalized to the histograms of the entire IR catalog.

sources with NIR matches. The fraction of sources with a match (shown in the right panel of Figure 6) is about 27 % for the X-ray sources with errors of 0.3″, and reaches nearly 90% around 1.1”. This implies that the sources with larger positional errors have more spurious matches, as would be expected.

2. Hardness ratios Soft X-rays are not expected to penetrate the gas and dust column to the Galactic Center. The X-ray hardness ratio provides a way to divide the X-ray sources into those that are heavily absorbed and therefore at or beyond the Galactic Center, or soft and therefore located well in front of the GC. We adopt the same hardness ratio criteria as in Muno et al. (2009). They define $HR0 = \frac{(h-s)}{h+s}$, where h is the flux in the 2.0-3.3 keV energy band and s is the flux in the 0.5-2.0 keV energy band. Soft sources are defined to have $HR0 < -0.175$. Any source with a $HR0 > -0.175$ or with no counts in the soft band are defined to be *hard* sources. Of the 4268 X-ray sources in our field, 3583 are *hard* and 685 are *soft*.

3. X-ray brightness We divide the X-ray catalog into *bright* and *faint* on the basis of the total count rate. The distribution of count rates shows a roughly Gaussian distribution

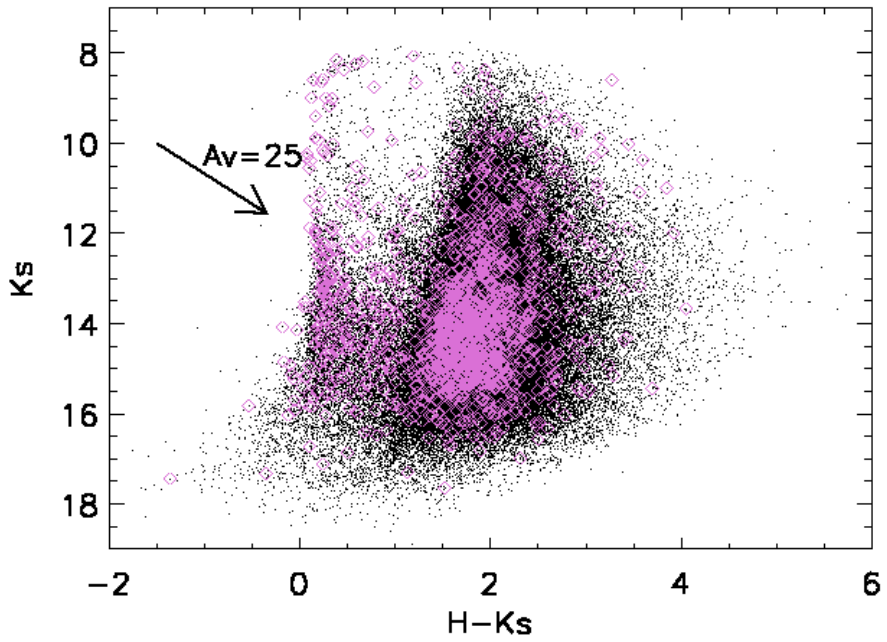

Fig. 4.— Color magnitude diagram of the ISPI catalog (in black) with candidate counterparts to *Chandra* X-ray sources marked in magenta.

with a tail toward the bright end. We define sources to be within this bright tail if their combined hard and soft count rate is greater than 1×10^{-4} photons $s^{-1}cm^{-2}$. There are 1075 sources brighter than this threshhold and 3193 fainter. We estimate the corresponding X-ray luminosity by assuming that the sources lie in the Galactic Center and using the *Chandra* proposal planning tool, *PIMMS*. Using a GC distance of 8kpc, a power law index of $\Gamma = 2.0$, and an absorbing column of $N_H = 6 \times 10^{22} cm^{-2}$, our bright/faint threshold corresponds to $L_X = 8 \times 10^{31}$ ergs/s for sources at the GC distance.

4. IR source density Dust lanes are evident in the image of the ISPI data in Figure 1. The lanes correspond to lines of sight with higher extinction and are seen as regions with more reddened colors and fewer star counts. We attempt to quantitatively locate these higher extinction areas by computing the average stellar surface density in the vicinity of the X-ray sources. We calculate the stellar surface density using stars with $10 < K_s < 13.5$ *mag* within a 10" radius of each X-ray source and normalize this value by Σ_{ISPI}, the mean density of $10 < K_s < 13.5$ *mag* stars in the entire ISPI GC field. Therefore the density parameter is the fraction of the mean density of the field. We call regions with $> 1.0 \times \Sigma_{ISPI}$, *dense* and regions with values $\leq 1.0 \times \Sigma_{ISPI}$, *sparse*. The intention is that *sparse* areas indicate

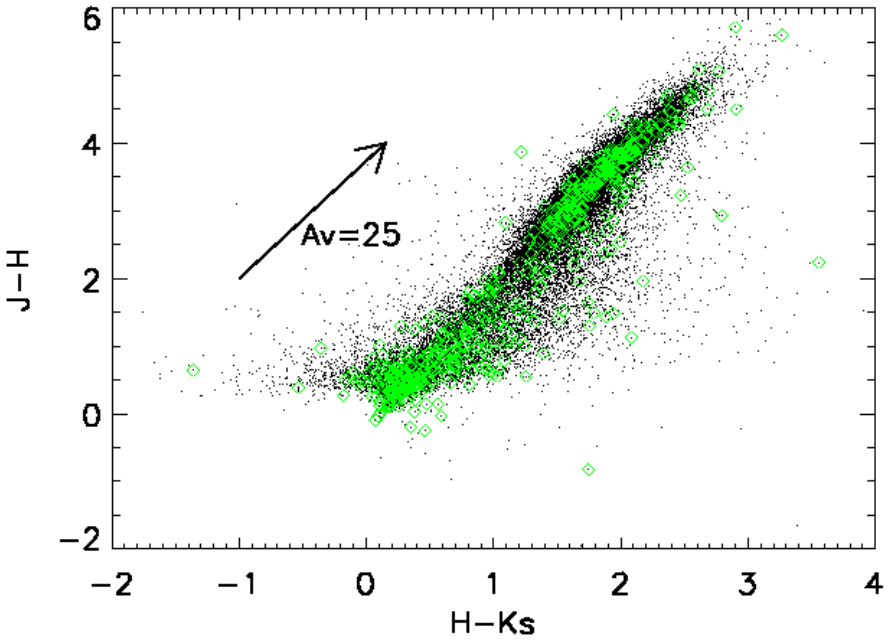

Fig. 5.— Color-color diagram of the ISPI catalog (in black) with candidate counterparts to *Chandra* X-ray sources marked in green.

regions of high extinction and *dense* areas indicate windows of lower extinction.

5. IR catalog properties The characteristics of the infrared catalog include the J, H and K_s magnitudes and the $J-H$, $J-K_s$, and $H-K_s$ colors. Two major populations can be seen in the $H-K_s$ distribution in Figure 7. There is a less reddened population, centered at $H-K_s = 0.2\ mag$ and a more reddened population centered at $H-K_s = 2.0\ mag$. We separate the two at $H-K_s = 1.0\ mag$, and call sources with $H-K_s < 1.0\ mag$, *unreddened* and sources with $H-K_s > 1.0\ mag$, *reddened*. We derived corresponding criteria for $J-H$ and $J-K_s$ using the Galactic bulge extinction ratios from Nishiyama et al. (2008). These were $J-H < 1.76\ mag$, $J-K_s < 2.76\ mag$ for *unreddened* sources and $J-H > 1.76\ mag$, $J-K_s > 2.76\ mag$ for *reddened* sources.

4.2. Estimating the number of spurious NIR matches to the *Chandra* catalog

We simulated the rate of false matches by performing Monte Carlo tests of the matching procedure. In this procedure, the positions of the ISPI NIR catalog sources are fixed while the

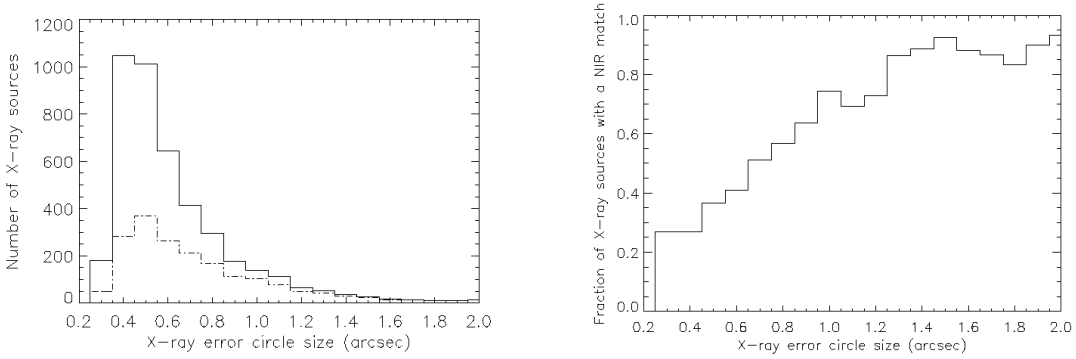

(a) (b)

Fig. 6.— (left) Distributions of positional error sizes of all 4268 *Chandra* X-ray sources in the ISPI GC field (solid line), and for the subset of these X-ray sources with one or more NIR matches (dashed line).(right) Fraction of X-ray sources with one or more NIR astrometric matches versus the X-ray positional error size.

positions of the 4268 X-ray sources with $\sigma_X \leq 2.0$" are randomly shifted. The X-ray sources are repositioned to lie between 0" and 10" of their original position in a random direction. All the other X-ray properties, including the positional error and X-ray photometry are preserved during the process. We performed the randomization 3,000 times, producing 3,000 artificial X-ray catalogs. Then we cross-correlated the artificial X-ray catalogs to the NIR catalog in the same way as for the original, positionally aligned X-ray catalog, using $\sigma_X + 0.2$" as the matching radius, in arcseconds. In the following, we call the X-ray catalog with the true X-ray source positions the *aligned* X-ray catalog.

The number of NIR-matched X-ray sources to the aligned X-ray catalog is called N_{obs} and the total number of X-ray sources in the catalog is A. The *average* number of IR-matched X-ray sources to the randomized catalogs is called N_{ran}, and the standard deviation of this number is called $\sigma_{N_{ran}}$. These variables can refer to the entire catalog of X-ray sources or to a subset with specified X-ray properties (for example, *soft* X-ray sources with *bright* X-ray flux, or *hard* X-ray sources with $\sigma_X \leq 0.5$").

The number N_{obs} includes both real physical matches and spurious matches. We would like to calculate the number of spurious matches, N_{spur} and subtract it from N_{obs} to obtain the number of real matches, N_{real}. However, the randomized X-ray catalogs consist of randomizations of *all* the X-ray sources, including the ones with true detected NIR counterparts. When randomized, these true matches contribute to the total N_{ran}, making it an *overestimate* of the number of spurious matches to the aligned X-ray catalog.

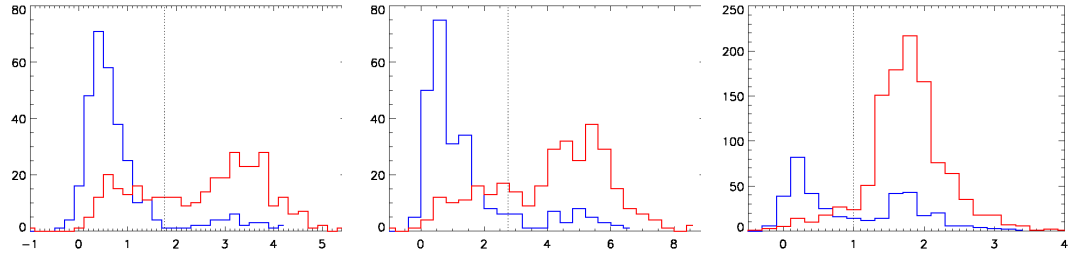

(a) $(J-H)$ *all matches* (b) $(J-K_s)$ *all matches* (c) $(H-K_s)$ *all matches*

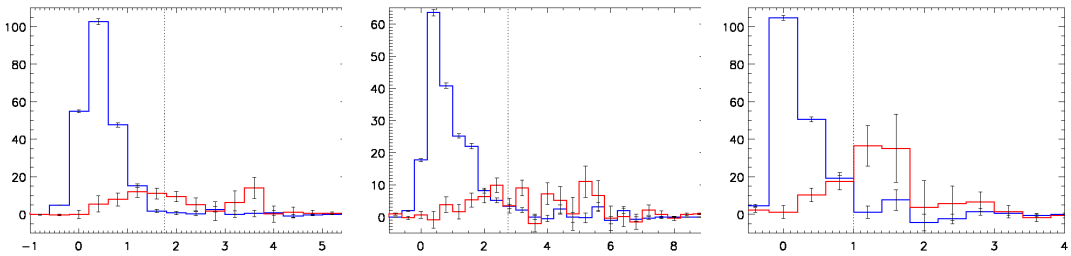

(d) $(J-H)$ *real matches* (e) $(J-K_s)$ *real matches* (f) $(H-K_s)$ *read matches*

Fig. 7.— Histograms of the infrared colors of matches to soft (blue histogram) and hard (red histogram) X-ray sources. Frames (a), (b) and (c) show the $J-H$,$J-K_s$ and $H-K_s$ distributions for *all* candidate counterparts and frames (d),(e) and (f) show the same color distributions for the estimated numbers of real counterparts (see Sections §4.5 and §4.6). The dotted lines indicate our cut between *unreddened* and *reddened* ISPI sources.

Fortunately, N_{real} can be solved in terms of the known values of N_{obs}, N_{ran} and A. The variable definitions are collected in Table 3.

From the definition of N_{obs}:

$$N_{obs} = N_{real} + N_{spur} \tag{1}$$

To represent N_{ran} in terms of our defined variables we assume that the randomized X-ray catalogs should contain 0 real NIR matches to the X-ray sources. We define the rate of spurious IR matches to the real X-ray catalog to be R. This rate is the number of spurious matches divided by the total number of X-ray sources *without* detected real NIR counterparts, i.e. $A - N_{real}$.

$$R = \frac{N_{spur}}{A - N_{real}} \tag{2}$$

If we assume that R is the same value for *all* the randomized X-ray catalogs, then N_{ran} is

simply, $A \times R$.

$$N_{ran} = A \times \frac{N_{spur}}{A - N_{real}} \tag{3}$$

When equations 1 and 3 are solved, we find that the number of real NIR matches within N_{obs} is:

$$N_{real} = N_{obs} - \frac{N_{ran}(A - N_{obs})}{A - N_{ran}} \tag{4}$$

and the number of spurious matches is

$$N_{spur} = \frac{N_{ran}(A - N_{obs})}{A - N_{ran}} \tag{5}$$

The uncertainty in these numbers is calculated by standard error propagation using the standard deviation of the number of matches from the random simulations, $\sigma_{N_{ran}}$.

$$\sigma_{N_{real}} = \sigma_{N_{spur}} = \frac{A^2 - AN_{obs}}{(A - N_{ran})^2}\sigma_{N_{ran}} \tag{6}$$

Table 3: Variable definitions for calculating numbers of real counterparts to X-ray sources, with unspecified IR properties

Variable name	Meaning
A	total num. of X-ray sources with a given set of X-ray properties
N_{obs}	num. of singly matched X-ray sources from aligned X-ray catalog
N_{ran}	mean num. of singly matched X-ray sources from rand. X-ray catalogs
$\sigma_{N_{ran}}$	standard deviation of N_{ran}
N_{real}	num. of *real* IR counterparts within N_{obs} matches
N_{spur}	num. of *spurious* IR counterparts within N_{obs} matches
$\sigma_{N_{real}}$	1σ error in value of N_{real}
$\sigma_{N_{spur}}$	1σ error in value of N_{spur}

We note that there are two critical assumptions for equations 1-6.

1) N_{obs} and N_{ran} contain only X-ray sources matched to a single IR counterpart. Our prescription omits the $\sim 6\%$ of X-ray sources with multiple matches, which obviously can also contain real X-ray/NIR counterparts. We address this omission in §5, where we use the rate of matches to real counterparts from these equations to estimate the number of additional real NIR counterparts present in the X-ray sources matched to multiple IR sources.

2) Equations 1-6 can only be used to find the numbers of real IR matches to X-ray sources *with specified X-ray properties*. The situation becomes more complicated if we wish

to find the number of X-ray sources that have real IR counterparts *with a specified IR property*. In these cases, the properties of the real NIR counterparts can bias the matching simulations. For example, we found that the number of soft X-ray sources matched to reddened IR counterparts was *higher* for the simulations than for the real X-ray catalog. This is because there is a number of real unreddened NIR counterparts to the soft X-ray sources, and when they are positionally randomized, they are more likely to be matched to reddened NIR sources, which make up ∼80% of the ISPI catalog. The solution is to rederive equations 1-6, keeping track of both the number of sources with and without the specified NIR property. This derivation is presented in *Appendix A*.

In the next section we briefly ignore the biases associated with the matching simulations in order to get an illustrative view of the content of the matched X-ray/NIR catalog. Then we apply these corrective equations in §4.5-4.6 and §6 to find more exact numbers of the real IR/X-ray counterparts.

4.3. The fractional excess of X-ray sources with NIR matches

We compare the fraction of matched X-ray sources in the Chandra catalog to the fraction obtained with the randomized catalogs. The randomized catalogs should contain essentially no true matches, so the difference between these two fractions will yield the fraction of X-ray sources with authentic detected matches in the ISPI catalog. Since this calculation does not address the overcounting of randomized catalog matches described in §4.2, the rates are all likely to be underestimates but they are useful to get an illustrative view of the level of real and spurious matching between the Chandra and ISPI catalogs.

We sort the X-ray catalog by the properties described in §4.1, including hard/soft, bright/faint and dense/sparse, and we count the number of sources with a specific set of properties that are matched to NIR sources. The size of the X-ray positional error circle is a strong factor in whether an X-ray source is matched, so we record the number of matched and unmatched sources per each X-ray positional error bin (σ_X is between 0.3" and 2.0" in intervals of 0.1"). We call the number of matched sources per error bin $N_{obs,i}$ where i is a label for the X-ray error circle size. The mean number of matched sources to the randomized X-ray catalogs is $N_{ran,i}$ and its standard deviation is σ_N. We divide $N_{obs,i}$,$N_{ran,i}$, and σ_N by A_i, the total number of X-ray sources in the Chandra catalog with the specified properties and error circle size. This yields the matching fractions $f_{obs,i}$ and $f_{ran,i}$ and the 1σ fractional scatter, $\sigma_{f,i}$. The fraction of X-ray sources (with a given σ_X) with a real detected counterpart is:

$$f_{real,i} = f_{obs,i} - f_{ran,i} \tag{7}$$

We combine the values of $f_{real,i}$ by calculating the weighted mean using $\sigma_{f,i}$ as the weight.

$$f_{real} = \frac{\sum_i \frac{f_{obs,i} - f_{ran,i}}{\sigma^2_{f,i}}}{\sum_i \frac{1}{\sigma^2_{f,i}}} \tag{8}$$

i is a label for the X-ray positional error bins (e.g. $i = 1, 2, 3... \Rightarrow \sigma_X = 0.3", 0.4", 0.5"...$)

The formal uncertainty of this expression is:

$$\sigma_f = \sqrt{\frac{1}{\sum_i \frac{1}{\sigma^2_{f,i}}}} \tag{9}$$

Table 4: Relative matching fraction for X-ray sources

Criteria	$f_{real} \pm \sigma_f$	Significance
All X-ray sources	0.052 ± 0.007	7.7σ
Soft sources	0.22 ± 0.02	13.6σ
Hard sources	0.016 ± 0.007	2.2σ
Soft, faint sources	0.15 ± 0.02	8.0σ
Soft, bright sources	0.42 ± 0.03	13.3σ
Soft sources, dense regions	0.18 ± 0.02	8.3 σ
Soft sources, sparse regions	0.23 ± 0.02	10.4 σ
Hard, faint sources	0.001± 0.008	0.2σ
Hard, bright sources	0.05 ± 0.01	3.8σ
Hard sources, dense regions	0.012± 0.009	1.4 σ
Hard sources, sparse regions	0.02 ± 0.01	1.7 σ

In Table 4 we show the R_{real} values and uncertainties for combinations of the X-ray source properties. 22% of soft sources have detected matches in the ISPI catalog compared to only 1.6% of the hard sources. Both soft and hard sources show a bias toward detection of *bright* sources over *faint* sources, with a *bright* source being more than twice as likely to have a detected counterpart.

There is a slight ($6\% \pm 3\%$) bias toward detecting soft sources in *sparse* regions over *dense* regions. This effect may be caused by the crowding limits being more severe in *dense* regions. There is no significant difference between *dense* and *sparse* regions seen in the hard

sources. However, the low number statistics for hard sources would mask an effect of similar magnitude to the soft sources.

The main point to draw from this is that hard sources have a particularly low rate of IR detection in the data, at least 4 times lower than for soft sources. We conclude that most of the sources in the X-ray catalog are too faint in the NIR to be detected by the ISPI observations, which is consistent with the finding that 57% of X-ray sources do not have a candidate match at all. We discuss the charactistics of the sources without NIR matches in the next section.

4.4. Characteristics of the X-ray sources without NIR matches

57 % of the X-ray catalog sources have no astrometric matches in the ISPI catalog. Soft X-ray sources have an unmatched percentage of 31% (214 unmatched out of 685 total soft X-ray sources) and hard X-ray sources have an unmatched percentage of 62% (2211 unmatched out of 3583 total hard X-ray sources).

The unmatched sources are skewed toward having smaller error circles compared to the total X-ray catalog. Their mean error circle size is 0.55" compared to 0.77" for the matched sources. We expect sources with smaller error circles to be less likely to have chance astrometric matches.

We find no difference in the X-ray brightness distributions of the unmatched X-ray sources and total catalog. However, we do find that the mean IR density in the vicinity of unmatched sources is *higher* than for the entire catalog. The mean stellar surface density around unmatched X-ray sources is $1.6 \times \Sigma_{ISPI}$, compared to $1.46 \times \Sigma_{ISPI}$ for the entire X-ray catalog. The effect is probably due to the fact that the smallest error circles with the lowest probability of chance matches lie in the center of the field where the stellar density is highest. For sources with $\sigma_X \leq 0.5$" and $\sigma_X > 0.5$", the mean densities are $1.8 \times \Sigma_{ISPI}$ and $1.0 \times \Sigma_{ISPI}$, respectively. Stellar density should have a linear effect on the chance for a spurious match, but the radius of the X-ray error circle should have a quadratic effect. Thus, it is predictable that the sources in the densest areas are also the most frequently unmatched.

We demonstrated in §4.3 that most of the astrometrically matched X-ray sources are spurious matches which means that either the source is too faint to be detected at all or it is blended with the brighter source or sources to which they are coincidentally matched. The unmatched sources can be useful because we know that in most cases their magnitudes are fainter than the ISPI data's detection limit. The ISPI detection limit varies with crowding

conditions but for this discussion we adopt the mean 50% completeness limits from artificial star tests in Table 1, which are $J = 18.4\ mag$, $H = 16.4\ mag$ and $K_s = 14.5\ mag$.

The unmatched soft sources are likely to be coronally active late type stars (Muno et al. 2003a). Coronal activity at the $> 10^{27}$ ergs/s level is seen at all spectral types in field dwarf stars (Feigelson 2004). For an illustrative case, we consider that a $J = 9\ mag$ M0 V star with no extinction would be detected in our ISPI data out to a distance of $\sim$ 800pc. Muno et al. (2003a) determine that the soft sources in the *Chandra* GC data can reside as far out as 4kpc, which leaves a substantial volume for coronally active late type dwarf stars to reside and yet be undetectable in our ISPI imaging.

The unmatched hard X-ray sources have a number of diverse candidates: AGNs, isolated pulsars and magnetars, magnetic CVs and LMXBs. Muno et al. (2003a) calculate that the $17' \times 17'$ central GC field should have between 20 and 100 AGN contributing to the hard source counts. AGN that are seen through the GC will be very faint. Bandyopadhyay et al. (2005) note that there are no AGN in the *Hubble* Deep Field North survey brighter than $K = 17\ mag$. After $A_K > 2.5\ mag$ extinction is added on, this magnitude is well beyond our sensitivity, which means that there should be no detected counterparts for the $\sim 10^2$ AGN in the X-ray catalog.

Isolated neutron stars can be bright at very young ages, but except for the Crab Pulsar, the brightest K band detected neutron star is the magnetar 1E 1547.0-54.08 with $K = 18.2\ mag$, at a distance of 9 kpc (Mignani 2009). We conclude that for all but the most exceptional systems, isolated pulsars in the GC should be undetectable in our ISPI data.

LMXBs and magnetic CVs share the same types of donor stars, usually late type K dwarfs (Jonker and Nelemans 2004; Knigge 2006). When in quiescence, these systems can be dominated by the light of the secondary star. In the case of a K0 dwarf star, a system in the Galactic Center would be $K \sim 21\ mag$, assuming $A_K = 2.5\ mag$ (Baganoff et al. 2003) and a GC distance of 8kpc (Gillessen et al. 2009; Cox 2000; Carroll and Ostlie 1996). Thus, the majority of canonical LMXBs and CVs would be undetected at GC distances in our ISPI data.

4.5. Probable matches to soft X-ray sources

The fraction of soft sources that are matched in section §4.3, suggests that a relatively high number of soft source candidate counterparts are real. We use the results of the random matching simulations with Equations 4 and A3 to derive the numbers of real counterparts to soft sources. We break down the soft X-ray/IR matches by source properties in Table 5.

There are 387 single IR matches to X-ray soft sources. Analysis of the randomized X-ray catalog matching suggests that 230 ± 12 are probable real matches, for a rate of $60 \pm 3\%$. We see that almost all (96%) the soft X-ray sources matched to unreddened NIR sources with a J detection are real, while a trivial number of matches to reddened X-ray sources are real. The lack of true soft/reddened sources is not surprising, because the X-ray attenuation implied by the reddened IR colors should make an intrinsically soft source be detected as a hard source, or be completely extinguished.

Table 5: Matching statistics for soft X-ray sources matched to a single IR source

Criteria	N_{obs}	N_{ran}	N_{real}	$R = \frac{N_{real}}{N_{obs}}$	σ_R	$\frac{R}{\sigma_R}$
All soft X-ray	387	236.0	230	0.60	0.03	18.5
Unreddened	254	45.9	224	0.88	0.02	47.0
Reddened	133	190.1	7	0.05	0.08	0.6
With J detection	286	47.8	254	0.89	0.02	51.2
With no J detect.	101	188.1	-24	-0.24	0.11	2.2
Unred. with J det.	242	15.5	232	0.96	0.01	87.1
Red. with J det.	44	32.4	22	0.51	0.09	5.6

4.6. Probable matches to hard X-ray Sources

There are 1223 hard X-ray sources with only a single NIR candidate counterpart in our ISPI catalog. However, when the randomized X-ray catalogs are matched to the ISPI catalog, 1135.0 matches are created on average, meaning a large percentage of hard, matched sources are spurious. Our analyses indicate that the number of real physical associations within the 1223 matches is 129 ± 39 sources, or $11\% \pm 3\%$ (see Table 6). Such a low rate of true matches is a problem for observing campaigns that seek to followup these sources. We therefore try to find the source parameters that maximize the return rate. In particular we wish to locate probable real matches which are both hard and reddened, which would suggest that they exist at or beyond the Galactic Center distance. We present the statistics for a number of properties and combinations of properties in Table 6.

The most promising property seems to be whether or not a candidate counterpart has a J-band detection. In Table 6, we see that there are 96 ± 35 probable true matches within the set of 1004 NIR single reddened/hard X-ray matches. 51 ± 13 of these probable true matches are among the 216 candidate matches with a J-band detection, meaning the remaining 45 true matches are among the 788 candidate matches without a J-band detection. Even though

the number of probable true matches within the J detected and J undetected categories are roughly the same, the percentage of candidate matches that are real clearly favors those with J-band detections: $27 \pm 5\%$ for J detected versus $6 \pm 4\%$ for J undetected.

With this in mind, we break the set of J band detected hard and reddened matches into sub-catagories of *bright/sparse*, *bright/dense*, *faint/sparse* and *faint/dense*. X-ray sources which are *bright* include 76 single source IR matches and have a 45 % probability of being real. If we restrict the error circle sizes of the X-ray sources to $\sigma_X \leq 1.0$, the number of true IR matches drops by 1 source, and the probability of being real rises to 47% (see second-to-last row of Table 6). The X-ray faint sources with J band detections have a lower rate of expected real matches, 12%. We searched for other parameters that can raise the percentage of true sources within the X-ray faint category, and we find that if the sources are matched to $13.0 \leq K_s < 14.0$ *mag* IR sources (in addition to their being reddened and detected in the J-band), and the X-ray error circles are restricted to $\sigma_X \leq 1.0$, the percentage probability of being real rises to 40% (see last row of Table 6). The $13.0 \leq K_s < 14.0$ *mag* criterion is suggested by the color-magnitude analysis in §6.2. In combination, these two categories, shown in the bottom two lines of Table 6, have 98 X-ray/NIR candidate matches, with 44 ± 7 probable real matches.

In Figure 7 we plot the *J-H*, *J-*K_s and *H-*K_s histograms for all the candidate matches followed by the color histograms for the component of the matches that are expected to be real. The numbers of soft source matches are shown in blue and the hard source matches are shown in red. It is apparent that the ratio of real to candidate sources is much higher for soft sources than hard sources. Also, soft sources with reddened counterparts seem to nearly all be spurious, as are most hard sources with unreddened counterparts.

5. Total number of real counterparts in the ISPI catalog

There are 233 X-ray sources with 2 or more NIR candidate counterparts in the matched catalog, totalling 527 matches. Of these 233 sources, 84 are X-ray soft (with 185 matches) and 149 are X-ray hard (with 342 matches). We use the rate of real matches, $R = N_{real}/N_{obs}$ derived in §4.5 and 4.6 and listed in Tables 5 and 6 to estimate the total number of detected true NIR counterparts within the multiply matched sources.

Table 6: Matching statistics for hard X-ray sources matched to a single IR source

Criteria	N_{obs}	N_{ran}	N_{real}	$R = \frac{N_{real}}{N_{obs}}$	σ_R	$\frac{R}{\sigma_R}$
All hard X-ray	1223	1135.0	128	0.11	0.03	3.3
Unreddened	219	193.1	33	0.15	0.06	2.4
Reddened	1004	941.9	96	0.10	0.04	2.7
With J detection	310	233.5	85	0.27	0.05	5.4
With no J detect.	913	901.6	44	0.08	0.05	1.3
Unred. with J det.	94	62.5	34	0.36	0.08	4.4
Red. with J det.	216	171.0	51	0.24	0.06	3.9
X-ray bright sources	324	270.2	66	0.20	0.05	4.2
X-ray faint sources	899	864.8	82	0.09	0.06	1.5
Dense regions	801	748.4	76	0.10	0.04	2.4
Sparse regions	422	386.7	53	0.13	0.05	2.3
Bright,red., w/ J	76	45.0	34	0.45	0.08	5.3
Faint, red., w/ J	136	121.9	16	0.12	0.08	1.5
Dense, red J	166	131.6	39	0.23	0.07	3.3
sparse red J	50	39.4	12	0.25	0.12	2.0
bright dense red w/ J	54	34.8	22	0.41	0.10	3.9
bright sparse red w/ J	23	12.3	12	0.51	0.14	3.5
faint dense red w/ J	112	96.7	17	0.15	0.09	1.6
faint sparse red w/ J	27	27.0	1	0.03	0.19	0.1
bright, red. w/ J, $\sigma_X \leq 1.0$	69	39.7	32	0.47	0.09	5.5
faint, red. w/ J, $\sigma_X \leq 1.0$, $13.0 \leq K_s < 14.0$,	29	17.6	12	0.40	0.14	2.8

5.1. Soft sources

The real counterpart matching rate for soft X-ray sources is 0.60 ± 0.032, as derived from the singly matched sources. When applied to the 84 multiply matched soft X-ray sources, we expect an additional 50 ± 2 real counterparts. However, a stronger predictor of real matches is the presence of a J band detection. Within these 84 sources, 66 have a J detected counterpart. If we apply the rate of real matches for J-detected soft source counterparts of 0.89 ± 0.017 we estimate 59 ± 1 real matches within the multiply-matched soft sources. The 18 soft sources with no J band counterpart have no expected real matches. Thus, if we include singly and multiply matched soft X-ray sources, we expect there to be $230 + 59 = 289 \pm 13$ real IR counterparts to soft sources in our ISPI catalog. The fraction

of soft sources with detected counterparts is $f_{real} = \frac{289}{685} = 0.42 \pm 0.02$.

In the ISPI $17' \times 17'$ area, Mauerhan et al. (2009) find 324 candidate matches to soft X-ray sources; 200 of these are unreddened. They do not report on the probable number of true matches within this field, but they find that within the entire $2^\circ \times 0.8^\circ$ field, 890 out of 1007 blue matches are real. If the ratio of 0.88 holds for the $17' \times 17'$ subfield, then they discovered ~ 177 unreddened real counterparts to soft X-ray sources in the $17' \times 17'$ ISPI GC field. They report essentially zero real reddened soft source counterparts making their total detected fraction of soft X-ray counterparts, $f_{real} \sim \frac{177}{685} = 0.26$. Our value of 0.42 ± 0.02 is larger, which we expect because our catalog has twice as many detected sources as the SIRIUS catalog within this area due to our NIR data's greater depth and resolution.

5.2. Hard sources

For hard sources, the rate of real counterparts to number of candidate counterparts is 0.11 ± 0.03, for an estimated total of 16 ± 5 within the set of 149 hard sources with multiple matches.

To get a better estimate of the real counterpart content of the multiply matched sources we break this set into the following criteria:

1) *hard* reddened sources with J band detections (24% real matches)

2) *hard* unreddened sources with J band detections (37% real matches)

3) *hard* reddened sources *without* J band detections (6% real matches)

4) *hard* unreddened sources *without* J band detections (0% real matches)

In parentheses is the fraction of real matches to candidate matches calculated for singly matched sources in Table 6. Since these sources are multiply matched, it is possible for an X-ray source to have a match for more than one of criteria 1-4.

To reduce the complexity we note that the real match probability for X-ray sources with J band detected matches is much higher than for X-ray sources without J band detected matches. Therefore, we assume that if one of these multiply matched hard sources has a J detected counterpart, the possibility that any additional matche without a J detection is the real counterpart is negligible.

There are 65 multiply matched hard X-ray sources with at least one J detected match. Four(4) have both unreddened and reddened J band detected matches, 28 have reddened J band detected matches and 33 have unreddened J band detected matches. For the 4 sources

with both reddened and unreddened matches, we estimate 0.4 ± 0.1 real reddened matches and 0.9 ± 0.2 real unreddened matches. The 28 X-ray sources with reddened J band matches should contain 7 ± 2 real matches and the 33 X-ray sources with unreddened J detected matches should have 12 ± 3 real matches.

The remaining sources 84 sources do not have J detections. Since we expect 0% of the unreddened sources without J detections to have matches, we only consider the subset of 76 X-ray sources with reddened candidate matches. Using the real match probability of 0.06, we estimate an additional 4 ± 3 real reddened matches to hard X-ray sources from this set of sources.

In total, we find that there should be 24 ± 4 additional real matches to the 149 multiply matched hard X-ray sources. 11 ± 3 are reddened and 13 ± 3 are unreddened.

The total number of real, hard X-ray source counterparts for singly and multiply matched data is $129 + 24 = 153 \pm 39$ sources. 107 ± 37 sources are hard and reddened, and 44 ± 14 are hard and unreddened.

This amounts to a fraction of $f_{real} = \frac{153}{3583} = 0.04 \pm 0.01$ hard X-ray sources with detected counterparts. Mauerhan et al. (2009) found a rate of 0.058 ± 0.015 with data that is slightly shallower in depth but that spans a larger area around the GC; nevertheless, our fraction is still consistent with Mauerhan et al. (2009) within the errors.

For a fairer comparison, we use their statistics on the $8'$ radius region around Sgr A* ($\alpha = 266.41726$, $\delta = -29.00798$). They calculate the number of real hard reddened counterparts within this region to be 46.2 ± 23.1 sources out of 617 candidate matches.

Our total for this region is 73 ± 33 sources out of 1018 X-ray sources with candidate matches. This fraction is consistent with Mauerhan et al. (2009) and our greater total is likely due to the greater depth and resolution of the ISPI imaging with respect to the SIRIUS data.

6. CMD positions of probable real matches

We constructed an infrared color-magnitude diagram for probable real matches to X-ray sources. We divided the X-ray sources into soft and hard and then used the matching statistics within the $H - K_s/K_s$ CMD with equations A3 and A4 to locate color-magnitude regions where there are excess matches to the aligned X-ray catalog. We calculate the excess in matches using bins of 1 magnitude in K_s and 1 magnitude in $H - K_s$, ranging from $0.0 < H - K_s < 4.0\ mag$ and $8.0 < K_s < 17.0\ mag$. This approach has the advantage

that it does not exclude any region of the CMD a priori, as would happen if we forced a J detection or a color cut.

In Figures 8 and 9 we show the CMD of the entire ISPI catalog overplotted by boxes which are color-coded to represent the number of probable true counterparts within a CMD bin. Here we only include X-ray sources with a single IR match. The box colors are black, yellow, green and blue, and correspond to 0, $1-5$, $5-9$, and >9 real matches, respectively. Bins with less than a 2σ significance ($\frac{N_{real,1}}{\sigma_{N_real,1}} < 2.0$) are also marked in black.

6.1. CMD of soft source counterparts

In Figure 8 we see that the real soft sources are mostly confined to $H - K_s < 1\ mag$, and $8.0 < K_s < 16.0$ mag, with a small number in the bright but more reddened CMD bins ($H - K_s > 1\ mag$, and $9.0 < K_s < 12.0$ mag). The number of unreddened counterparts are consistent with the contribution expected from coronally active stars in the field (Mauerhan et al. 2009; Muno et al. 2009). The fact that the X-ray spectra appear soft suggests that these sources lie within 4 kpc of the sun (Mauerhan et al. 2009). Since the stars can be arbitrarily closer than this distance, and dwarf stars have a wide dispersion in magnitudes, it is difficult to place further constraints on the population of unreddened IR counterparts to soft X-ray sources without spectroscopy.

The real counterparts to soft sources with $H-K_s > 1\ mag$ are more mysterious since the high reddening implied by the IR color should also make the X-ray component appear hard. However, Mauerhan et al. (2009) do note that for sources near the hard/soft threshhold, the uncertainty could cause a hard source to be labeled as a soft source, and vice versa. Another possibility is that these systems may have internal absorption that affects the IR component more than the X-ray component. Finally, for some sources that are particularly strong soft X-ray emitters, the large extinction may not soften it enough to change its hard/soft designation. One such source in our sample (CXO174550.6-285919), is nominally soft and reddened but spectroscopic follow-up found that it was a Wolf-Rayet binary in the Galactic Center, with a spectral class WN6b (Mauerhan et al. 2010).

In §4.5 we found that 96% of the 242 singly matched soft X-ray source counterparts with unreddened colors and J detections are likely to be authentic. We plot their positions over the ISPI CMD in the right panel of Figure 8. However, because we used unreddened colors and a J band detection as a criteria in order to enhance the probability, any real reddened matches to soft X-ray sources will not represented in this figure.

6.2. CMD of hard source counterparts

The hard X-ray source CMD has three bins with a 2σ detection of 9 or more real matches (the blue boxes in Figure 9). All of these CMD bins reside in the $1 < H - K_s < 2\ mag$ column of the CMD. The magnitudes at which these appear are not contiguous, with 9 ± 3 sources at $10 < K_s < 11\ mag$, 23 ± 9 sources at $13 < K_s < 14\ mag$ and 21 ± 9 sources at $15 < K_s < 16\ mag$. There are also a handful of true counterpart detections in the unreddened bins dispersed between $10 < K_s < 16\ mag$ as well as 5 ± 1 likely true counterparts at $10 < K_s < 11\ mag$ and $3 < H - K_s < 4\ mag$.

In the right panel of Figure 9 we show the CMD positions of the 98 hard, reddened matches with a J-band detection, of which $\sim 45\%$ should be real as discussed in §4.6. These sources represent the highest proportion of reddened authentic counterparts to hard X-ray sources that we could locate in the matched catalog. Even so, half of these counterparts are spurious. Since the criterion of a J detection was used to enhance the real counterpart probability, the lower right CMD is excluded due to flux sensitivity.

The unknown distance, unknown extinction and unknown intrinsic $(H-K_s)_0$ color make interpretation of the hard counterpart CMD complicated. Nevertheless, a useful constraint on the M_{K_s} magnitudes can be found by considering ranges of the uncertainty in these parameters.

Muno et al. (2009) argue that the majority of hard X-ray sources must be farther than 4kpc from the Sun, because of the extinction column required to make soft sources appear as hard. We adopt this value as the minimum distance for hard X-ray sources. For the maximum distance, we use a value of 8kpc, a reasonable value for the distance to the Galactic Center. There is the possibility of observing bright IR counterparts on the far side of the bulge (with distance $> 8kpc$). However, the strongest candidate CMD bins lie in the $1 < H - K_s < 2\ mag$ range, which is mostly to the blue side of the modal value of $H - K_s = 1.8\ mag$ for the ISPI catalog, implying that they may lie on the near side of the GC.

The intrinsic colors for main sequence, giant and supergiant stars range from $-0.06 < (H - K)_0 < 0.36\ mag$, and $-0.06 < (H - K)_0 < 0.1\ mag$ for all spectral types except for M (Cox 2000). We use this dispersion in intrinsic color and the $1 < H - K_s < 2\ mag$ limits of the color bin to calculate the range in absolute K_s extinction, A_{K_s}. Using extinction ratios for the Galactic Center of $A_V : A_J : A_H : A_{K_s} = 1.00 : 0.188 : 0.108 : 0.062$ (Nishiyama et al. 2008) we find that sources with $1 < H-K_s < 2\ mag$ are experiencing $0.86 < A_{K_s} < 2.78\ mag$ of extinction.

We estimate the absolute M_{K_s} magnitude range for the blue bins in Figure 9 using

equation 10 with the magnitude ranges of the bins and the estimated A_{K_s} range.

$$M_{K_s} = K_s - 5log(d) + 5 - A_{K_s} \tag{10}$$

The resulting limits on M_{K_s} are listed in Table 7.

The ranges of possible M_{K_s} are broad: each 1 magnitude bin in apparent magnitude can accommodate an interval of $\sim 3\ mag$ in absolute magnitude for certain distances and extinctions. But we can still suggest certain classes of object that meet the criteria for these probable real sources.

The systems in the $10 < K_s < 11\ mag$ bin have a possible range of $-2.9 < M_K < -7.3\ mag$. The matched catalog contains 20 candidate matches in this bin, and 4 of these have had published spectroscopic followup. Mauerhan et al. (2010) observed K band spectra of the NIR counterparts to CXO174532.7-285617, CXO174536.1-285638, CXO174555.3-285126, CXO174617.0-285131 which all lie within the $10 < K_s < 11\ mag$, $1 < H - K_s < 2\ mag$ bin and are X-ray hard. They found spectral types of O4-6I, WN8-9h, WN5-6b, O6If+ respectively. Supergiants of all spectral types are brighter than $M_K \sim -6\ mag$, as are Wolf Rayet stars and O main sequence stars (Cox 2000; Carroll and Ostlie 1996). At the GC extinction levels, Wolf Rayet stars and single O stars are usually too soft in X-rays to be detected. However, if they exist in a binary, with either an accreting compact object or a star with high mass loss, then this can create a wind shock zone energetic enough to generate hard X-rays.

The sources in the $13 < K_s < 14\ mag$, $1 < H - K_s < 2\ mag$ bin should come from stars with $0.1 < M_K < -4.3\ mag$ and the $15 < K_s < 16\ mag$, $1 < H - K_s < 2\ mag$ bin sources correspond to $2.1 < M_K < -2.3\ mag$. Both ranges overlap well with giant stars in luminosity class III, which have $M_{K_s} = -0.75\ mag$ for G types and get monotonically brighter to $M_{K_s} = -5\ mag$ for mid M type giants (Carroll and Ostlie 1996; Cox 2000). These stars could produce the requisite hard X-rays if they belonged to an accreting binary system, such as a LMXB or a symbiotic binary (containing a RGB star and a white dwarf). Most symbiotic stars have soft X-ray spectra but recent evidence suggests that symbiotic stars with a highly magnetized white dwarf have hard X-ray spectra (Luna and Sokoloski 2007).

B0-B8 stars on the main sequence have $0 < M_{K_s} < -3\ mag$, which also makes them good candidates for the $13 < K_s < 14\ mag$ and $15 < K_s < 16\ mag$ bins. B star HMXBs are known to have hard spectra and would be expected to exist in regions where there has been recent star formation. This would be consistent with the known existence of young massive stars the GC.

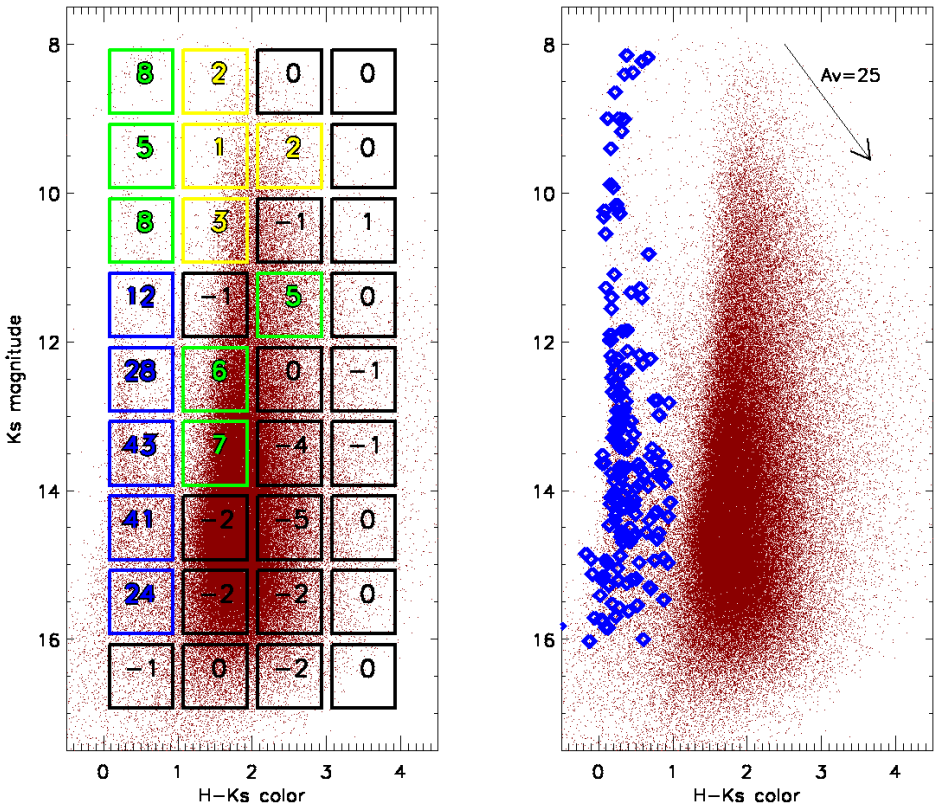

(a) (b)

Fig. 8.— (left) $H - K_s$, K_s color magnitude diagram of all ISPI sources, in red, with the positions of probable true counterparts to X-ray soft sources shown by the colored boxes. The color coding is yellow: 1-5 sources, green: 5-9 sources, and blue: 9 or more sources. Black boxes contain counts with lower than 2 σ significance and are consistent with 0 real counterparts. The boxes are undersized for clarity. (right) $H - K_s$, K_s color magnitude diagram of all ISPI sources, in dark red. Overplotted in blue are a set of 242 soft X-ray matches with J band detections and low reddening. These 242 IR sources should have a 96% likelihood of being the true counterparts to their matched X-ray sources. See §4.5 for details.

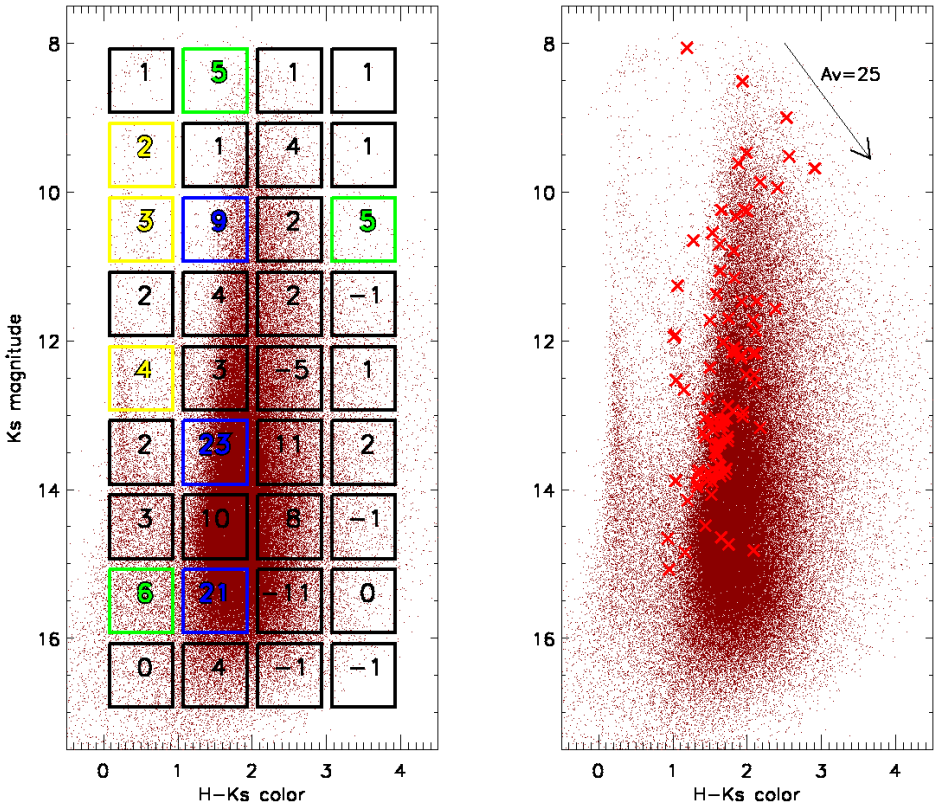

(a) (b)

Fig. 9.— (left) $H - K_s$, K_s color magnitude diagram of all ISPI sources, in red, with the positions of probable true counterparts to hard X-ray sources shown by the colored boxes. The color coding is yellow: 1-5 sources, green: 5-9 sources, and blue: 9 or more sources. Black boxes contain counts with lower than 2 σ significance and are consistent with 0 real counterparts. The boxes are undersized for clarity. (right) $H - K_s$, K_s color magnitude diagram of all ISPI sources, in dark red. Overplotted are a set of 98 hard X-ray matches with reddened colors, J band detections, small positional errors ($\sigma_X \leq 1.0$") and are either X-ray bright or X-ray faint with $13 \leq K_s < 14$ *mag*. These 98 IR sources should have a 45% likelihood of being true counterparts to their matched X-ray sources. See §4.6 for details.

7. Conclusions

We cross-correlated a new JHK_s catalog of the central $17' \times 17'$ of the Galaxy with a catalog of 9017 X-ray point sources observed with *Chandra*. Our catalog of astrometrically matched candidate counterparts contains 2137 IR matches to 1843 X-ray sources. Through Monte Carlo simulations of the matching precedure we determine that the candidate matches contain 289 ± 13 true matches to soft X-ray sources and 154 ± 39 true matches to hard X-ray sources. The soft X-ray sources are likely to be a mix of coronally active dwarf stars within 4 kpc, and we find that, by choosing the candidate singly matched 242 IR/X-ray candidate counterparts with unreddened infrared colors and J band detections, there will be 232 ± 2 real NIR counterparts.

Hard, reddened sources, which other authors have suggested to be a mix of HMXBs, colliding wind binaries and other rare systems in the Galactic Center vicinity, should have 110 ± 40 real infrared matches in our catalog, out of 1372 candidates. We calculate the difference in CMD diagrams between candidate matches and simulated spurious matches and locate 3 distinct regions of the $H - K_s/K_s$ CMD with a significant number of probable real counterparts. Hidden behind between $0.86 < A_{K_s} < 2.78$ mag of extinction, some of these sources should have absolute magnitude ranges compatable with Wolf-Rayet stars and supergiants, while the fainter two bins are more likely to be main sequence B star HMXBs or RGB stars with a compact accreting companion (possibly a neutron star or black hole LMXB or as a symbiotic star with a magnetic white dwarf).

The low probability ($\sim 10\%$) of finding real matches in the set of hard match candidates is a challenge for spectroscopic follow-up campaigns. We find sets of properties which enhance the probability of obtaining real matches to X-ray hard, IR-reddened sources. We find that by restricting the hard, reddened candidate matches to those that are X-ray bright, with positional errors $\sigma_X \leq 1.0$, and that are matched to an IR source with a J band detection, or from X-ray faint sources with small positional errors ($\sigma_X \leq 1.0$) with $13.0 \leq K_s < 14.0$ mag and a J band detection, one is likely to find 44 ± 7 real IR counterparts out of a total of

Table 7: Ranges of M_{K_s} possible for real sources in CMD bins from Figure 9. The color range is $1.0 < (H - K_s) < 2.0$ for all three bins.

Apparent magnitude range	M_{K_s} for $d = 4kpc$	M_{K_s} for $d = 8kpc$
$10 < K_s < 11$	$-5.8 < M_{K_s} < -2.9$	$-7.3 < M_{K_s} < -4.4$
$13 < K_s < 14$	$-2.8 < M_{K_s} < 0.1$	$-4.3 < M_{K_s} < -1.4$
$15 < K_s < 16$	$-0.8 < M_{K_s} < 2.1$	$-2.3 < M_{K_s} < 0.6$

98 candidate counterparts. These results will be used for target selection and slit design to maximize the return of upcoming NIR spectroscopic campaigns, such as the FLAMINGOS-2 Galactic Center Survey (Eikenberry 2008).

A. Appendix

In section §4.2 we derived equations that estimate the number of singly matched X-ray sources with real NIR counterparts for X-ray sources with a given set of X-ray properties. We wish to extend this analysis to ask the question, how many real NIR counterparts are there for a given set of X-ray properties *and NIR properties*?

In this case, there is a bias that occurs when a real NIR counterpart is randomized to match a NIR source with the opposite NIR properties.

We begin by defining P to be a set of NIR properties (such as being within a $(H - K_s)$ color interval or having a J band detection).

$N_{obs,1}$ is the number of singly matched X-ray sources in the aligned X-ray catalog whose counterparts fall within P. $N_{obs,2}$ is the number singly matched X-ray sources whose counterparts fall within the *complement* of P.

$N_{obs,1}$ and $N_{obs,2}$ consist of both real and spurious NIR matches.

$$N_{obs,1} = N_{real,1} + N_{spur,1} \tag{A1}$$

and

$$N_{obs,2} = N_{real,2} + N_{spur,2} \tag{A2}$$

We define $N_{ran,1}$ and $N_{ran,2}$ to be the average number of singly matched X-ray sources to the randomized X-ray catalogs whose counterparts are within P and the *complement* of P, respectively.

As in §4.2, we assume the spurious match rate from the aligned X-ray catalog is the same as for the randomized catalog, and we find $N_{ran,1}$ and $N_{ran,2}$ to be:

$$N_{ran,1} = A \times \frac{N_{spur,1}}{A - N_{real,1} - N_{real,2}} \tag{A3}$$

and for spurious matches to sources without property P:

$$N_{ran,2} = A \times \frac{N_{spur,2}}{A - N_{real,1} - N_{real,2}} \tag{A4}$$

The result is four linear equations and four unknown variables, $N_{real,1}$,$N_{spur,1}$, $N_{real,2}$ and $N_{spur,2}$. Solving via Gaussian elimination gives:

$$N_{spur,1} = \frac{N_{ran,1}(A - N_{obs,1} - N_{obs,2})}{A - N_{ran,1} - N_{ran,2}} \tag{A5}$$

$$N_{real,1} = N_{obs,1} - \frac{N_{ran,1}(A - N_{obs,1} - N_{obs,2})}{A - N_{ran,1} - N_{ran,2}} \tag{A6}$$

$$N_{spur,2} = \frac{N_{ran,2}(A - N_{obs,1} - N_{obs,2})}{A - N_{ran,1} - N_{ran,2}} \tag{A7}$$

$$N_{real,2} = N_{obs,2} - \frac{N_{ran,2}(A - N_{obs,1} - N_{obs,2})}{A - N_{ran,1} - N_{ran,2}} \tag{A8}$$

The errors in the expected number of real counterparts follow from the standard rules of error propagation.

$$\sigma_{N_{real,1}} = \sigma_{N_{spur,1}} = \sqrt{(\frac{(A - N_{ran,2})(A - N_{obs,1} - N_{obs,2})}{(A - N_{ran,1} - N_{ran,2})^2})^2 \sigma^2_{N_{ran,1}} + (\frac{N_{ran,1}(A - N_{obs,1} - N_{obs,2})}{(A - N_{ran,1} - N_{ran,2})^2})^2 \sigma^2_{N_{ran,2}}} \tag{A9}$$

$$\sigma_{N_{real,2}} = \sigma_{N_{spur,2}} = \sqrt{(\frac{(A - N_{ran,1})(A - N_{obs,1} - N_{obs,2})}{(A - N_{ran,1} - N_{ran,2})^2})^2 \sigma^2_{N_{ran,1}} + (\frac{N_{ran,2}(A - N_{obs,1} - N_{obs,2})}{(A - N_{ran,1} - N_{ran,2})^2})^2 \sigma^2_{N_{ran,2}}} \tag{A10}$$

The variable definitions for this derivation are collected in Table 8.

Table 8: Variable definitions for calculating numbers of real counterparts to X-ray sources with a given IR counterpart property

Variable name	Meaning
A	total num. of X-ray sources with a given set of X-ray properties
$N_{obs,1}$	num. of singly matched X-ray sources from aligned X-ray catalog w/ P
$N_{obs,2}$	num. of singly matched X-ray sources from aligned X-ray catalog w/o P
$N_{ran,1}$	mean num. of singly matched X-ray sources from rand. X-ray catalogs w/ P
$N_{ran,2}$	mean num. of singly matched X-ray sources from rand. X-ray catalogs w/o P
$\sigma_{N_{ran,1}}$	standard deviation of $N_{ran,1}$
$\sigma_{N_{ran,2}}$	standard deviation of $N_{ran,2}$
$N_{real,1}$	num. of *real* IR counterparts within N matches w/ P
$N_{spur,1}$	num. of *spurious* IR counterparts within N matches w/ P
$N_{real,2}$	num. of *real* IR counterparts within N matches w/o P
$N_{spur,2}$	num. of *spurious* IR counterparts within N matches w/o P
$\sigma_{N_{real,1}}$	1σ error in value of $N_{real,1}$
$\sigma_{N_{spur,1}}$	1σ error in value of $N_{spur,1}$
$\sigma_{N_{real,2}}$	1σ error in value of $N_{real,2}$
$\sigma_{N_{spur,2}}$	1σ error in value of $N_{spur,2}$

REFERENCES

Arendt, R.G. et al. ApJ, 685, 958

Baganoff, F.K. et al. 2003, ApJ, 591, 891

Bandyopadhyay, R.M. et al. 2005, MNRAS, 364, 1195

Belczynski, K. and Taam, R.E. 2004, ApJ, 616, 1159

Carroll, B.W. and Ostlie, D.A. *An Introduction to Modern Astrophysics*, Addison-Wesley Publishing Company, New York, 1996, pp. A-13 - A-18.

Clark, J.S., Crowther, P.A. and Mikles, V.J. 2009, A&A, 507, 1567

Cox, A.N. *Allen's Astrophysical Quantities*, Springer-Verlag, New York, 4th Edition, 2000, pp. 151-153.

Eikenberry, S.S. 2008, AIP Conf. Proc., 1010, 132

Feigelson, E.D., et al. 2004, ApJ, 611, 1107

Gillessen, S., Eisenhauer, F.,Trippe, S.,Alexander, T.,Genzel, R.,Martins, F.,Ott, T. 2009, ApJ, 692, 1075

Gosling, A.J., Bandyopadhyay, R.M. & Blundell, K.M. 2009, MNRAS, 394, 2247

Gosling, A.J., Bandyopadhyay, R.M. & Blundell, K.M. 2010, MNRAS, *submitted*

Grimm, H.J., Gilfanov,M., and Sunyaev,R. 2003, MNRAS, 339, 793

Grindlay, J.E. et al. 2005, ApJ, 635, 920

Hodgekin, S.T., Irwin, M.J., Hewett, P.C. and Warren, S.J. 2009, MNRAS, 394, 675

Hyodo, Y., et al. 2008, PASJ, 60, 173

Jonker, P.G. and Nelemans, G. 2004, MNRAS, 354, 355

Knigge, Christian. 2006, MNRAS, 373, 484

Lawrence, A. et al. 2007, MNRAS, 379, 1599

Laycock, S., et al. 2005, ApJ, 634, L53

Lucas, P.W. et al. 2008, MNRAS, 391,136

Luna, G.J.M. and Sokoloski, J.L. 2007, ApJ, 671, 741

Mauerhan, J.C., Muno, M.P., and Morris, M. 2007, ApJ, 662, 574

Mauerhan, J.C., et al. 2009, ApJ, 703, 30

Mauerhan, J.C., et al. 2010, ApJ, 710, 706

Mignani, R.P. 2009, The Messenger, 138, 19

Mikles, V.J., Eikenberry, S.S., Muno, M.P., Bandyopadhyay, R.M., and Patel, S. 2006, ApJ, 651,408

Mikles, V.J., Eikenberry, S.S., Bandyopadhyay, R.M., and Muno, M.P. 2008, ApJ, 689,1222

Muno, M. P., et al. 2003, ApJ, 589, 225

Muno, M. P., et al. 2003, ApJ, 599, 465

Muno, M. P., et al. 2004, ApJ, 613, 1179

Muno, M. P., Bauer, F.E., Bandyopadhyay, R.M. and Wang, Q.D. 2006, ApJS, 165,173

Muno, M. P., et al. 2009, ApJS, 181, 110

Nishiyama, S., et al. 2008, ApJ, 680, 1174

Pfahl, E., Rappaport, S. and Podsiadlowski, P. 2002, ApJ, 571, L37

Skrutskie, M.F. et al. 2006, AJ, 131,1163

Stetson, P.B. 1987, PASP, 99,191

Tan, J.C, and Draine, B.T. 2004, ApJ, 606, 296

van der Bliek,N.S. et al. 2004, Proc. SPIE, 5492, 1582

Wang, Q.D., Gotthelf, E.V. and Lang, C.C. 2002, Nature, 415, 148

Warner, C., Gonzalez, A., Eikenberry, S.S. 2010, PASP, *in prep.*

Table 9. Sample Data of ISPI/Chandra matched sources catalog

X-ray ID	X-ray RA (deg)	X-ray DEC (deg)	σ_X (")	Source type	ISPI RA (deg)	ISPI DEC (deg)	J	J error	H	H error	K_s	K_s error
174457.1-285740	266.23813	-28.96121	1.8	hard	266.238118	-28.961	14.54	0.034	12.98	0.037	11.60	0.043
174457.4-285622	266.23941	-28.93967	2.0	hard	266.239377	-28.940386	18.09	0.069	14.01	0.043	12.74	0.051
-	-	-	-	-	266.239183	-28.939192	17.81	0.064	14.01	0.043	11.89	0.044
174459.9-290324	266.24982	-29.05683	2.0	hard	266.249972	-29.056337	13.66	0.031	13.06	0.037	11.20	0.041
174459.9-290538	266.24994	-29.09415	1.5	soft	266.250792	-29.094179	15.57	0.039	12.18	0.034	11.70	0.043
174500.2-290057	266.25113	-29.01598	2.6	hard	266.25107	-29.015537	14.87	0.035	12.52	0.035	10.83	0.039
174501.9-285719	266.25827	-28.95553	1.8	hard	266.258535	-28.955952	14.44	0.033	13.02	0.037	12.40	0.048
174502.2-285749	266.25946	-28.96381	1.0	hard	266.259295	-28.963779	14.11	0.032	11.75	0.033	10.41	0.038
174502.4-290205	266.26007	-29.03492	1.1	hard	266.259337	-29.03475	13.95	0.032	11.89	0.033	9.83	0.037
-	-	-	-	-	266.260048	-29.034872	13.84	0.031	11.93	0.033	9.98	0.037
174502.4-290453	266.26039	-29.0816	1.4	soft	266.260307	-29.081633	15.47	0.038	13.04	0.037	11.31	0.041
174502.8-290429	266.26198	-29.0748	1.3	hard	266.261948	-29.074818	13.41	0.030	12.93	0.037	12.76	0.052
174504.2-290410	266.26764	-29.06977	1.5	hard	266.268021	-29.070093	15.42	0.038	11.62	0.033	9.75	0.036
174504.2-290610	266.26841	-29.10258	1.9	soft	266.268758	-29.102386	16.39	0.046	12.31	0.034	10.78	0.039